

# Feasibility of control of particle assembly by dielectrophoresis in liquid-cell transmission electron microscopy

Tomoya Yamazaki<sup>1,\*</sup>, Hiromasa Niinomi<sup>2</sup> and Yuki Kimura<sup>1</sup>

<sup>1</sup>Institute of Low Temperature Science, Hokkaido University, Sapporo, Hokkaido, Japan

<sup>2</sup>Institute of Multidisciplinary Research for Advanced Materials, Tohoku University, Sendai, Miyagi, Japan

\*To whom correspondence should be addressed. E-mail: [yamazaki@lowtem.hokudai.ac.jp](mailto:yamazaki@lowtem.hokudai.ac.jp)

## Abstract

Liquid-cell transmission electron microscopy (LC-TEM) is a useful technique for observing phenomena in liquid samples with spatial and temporal resolutions similar to those of conventional transmission electron microscopy (TEM). This method is therefore expected to permit the visualization of phenomena previously inaccessible to conventional optical microscopy. However, dynamic processes such as nucleation are difficult to observe by this method because of difficulties in controlling the condition of the sample liquid in the observation area. To approach this problem, we focused on dielectrophoresis, in which electrodes are used to assemble particles, and we investigated the phenomena that occurred when an alternating-current signal was applied to an electrode in an existing liquid cell by using a phase-contrast optical microscope (PCM) and TEM. In PCM, we observed that colloidal particles in a solution were attracted to the electrodes to form assemblies, that the particles aligned along the electric field to form pearl chains and that the pearl chains accumulated to form colloidal crystals. However, these phenomena were not observed in the TEM study because of differences in the design of the relevant holders. The results of our study imply that the particle assembly by using dielectrophoretic forces in LC-TEM should be possible, but further studies, including electric device development, will be required to realize this in practice.

**Key words:** liquid-cell transmission electron microscopy, dielectrophoresis, particle assembly, *in situ* observation, electrodes, alternating current electric field

## Introduction

Liquid-cell transmission electron microscopy (LC-TEM), in which a volatile liquid sample is separated from a vacuum by electron-transparent membranes, is a technique that permits the dynamic visualization of various phenomena in liquids by TEM [1]. Although the spatial resolution of LC-TEM depends on the material, the liquid thickness and the electron dose rate, resolutions of less than 1 nm can be achieved [2], which is beyond that achievable optical microscopy governed, as it is, by the diffraction limit of visible light. The phenomena that can be visualized include nucleation, i.e. the formation of thermodynamically stable nuclei through unstable clustering of molecules at a nanoscale. Because nucleation is a nanoscale process, it cannot be visualized by optical microscopy, whereas electron microscopy, with its atomic spatial resolution, should be capable of visualizing the moment of nucleation. LC-TEM has already been used to capture the moment of crystal formation not only of metals [3,4] but also of calcium carbonates [5,6], protein crystals [7], organic crystals [8], metal–organic frameworks [9] and nanoprisms [10] among others. Some of these results suggest that intermediate metastable phases, such as amorphous phases, play an important role in the early stages of the formation of stable crystalline phases, opening the door to the unveiling of nucleation mechanisms.

On the other hand, it is still exceedingly difficult to capture the moment of nucleation by LC-TEM for several reasons. First, because nucleation is a spatiotemporally stochastic phenomenon, it is difficult to predict exactly where and when it will occur. Second, an increase in the magnification is generally required to observe nucleation in detail; this inevitably reduces the size of the field of view, leading to a lower probability of capturing the nucleation event. Finally, the most important issue to be resolved is the inability to control the local conditions necessary to induce nucleation within the field of view.

The basic strategy for promoting nucleation from a solution is to increase its supersaturation, which is expressed as  $\sigma = C/C_e$ , where  $C$  is the concentration of the solute and  $C_e$  is its solubility. Because the solubility depends on the temperature, it is a common practice to control the degree of supersaturation by means of precise temperature regulation at around room temperature when investigating crystallization by optical microscopy. However, precise control of temperature around the sample is difficult to achieve in TEM because of technical issues; although the technology for TEM holders in which the temperature can be controlled in the cryogenic and high-temperature regions has matured, the technology required for precise control ( $\pm 0.1^\circ\text{C}$ ) of temperatures near room temperature, especially in the cooling direction, is still

Received 2 December 2021; Revised 23 March 2022; Editorial Decision 19 April 2022; Accepted 20 April 2022

© The Author(s) 2022. Published by Oxford University Press on behalf of The Japanese Society of Microscopy.

This is an Open Access article distributed under the terms of the Creative Commons Attribution-NonCommercial License

(<https://creativecommons.org/licenses/by-nc/4.0/>), which permits non-commercial re-use, distribution, and reproduction in any medium, provided the original work is properly cited. For commercial re-use, please contact [journals.permissions@oup.com](mailto:journals.permissions@oup.com)

under development. It is therefore highly desirable to establish a method for precisely controlling local conditions to promote nucleation at the scale of the field of view of LC-TEM.

Currently, one effective method for changing the local supersaturation in the observation field in LC-TEM is through radiolysis by an electron beam. Radiolysis in LC-TEM involves the generation of radicals from the solvent driven by the energy of the electron beam. These radicals produce secondary chemical reactions that can change the composition of the solution in the field of view [11,12]. These electron-beam-induced radiolysis processes can often promote crystallization [3,8,13,14]. The overall process of radiolysis can be complex to understand, but two processes can generally promote crystallization: (i) reduction of metal ions to solids by hydrogen radicals or aqueous electrons [3] and (ii) the production of ions that are not present under the initial conditions. When the concentration of an ion increases through an accumulation of the electron dose, the substance related to the newly formed ion becomes supersaturated and crystallization can occur. Such processes have been observed in the crystallization of sodium sulfate [13] and sodium chloride [14]. However, this type of behavior is only possible under certain limited conditions.

How might we induce nucleation within an LC-TEM observation field for a wider range of materials? If molecules or particles could be assembled locally so as to increase their concentration, it might be possible to produce conditions of high supersaturation in which nucleation would be induced to occur within the LC-TEM observation field. One possible approach might be to use dielectrophoresis (DEP) to assemble relatively large particles, such as protein molecules or colloidal particles. This technique does not assemble ions such as  $\text{Na}^+$  and  $\text{Cl}^-$ , which are added as salting agents to control the solubility of protein crystals. Consequently, the supersaturation of protein crystals could be increased without changing the solubility. DEP is defined as the relative motion of a suspended particle and a solvent resulting from polarization forces produced by an inhomogeneous electric field [15]. The resultant force  $F_{DEP}$  can be expressed as follows [16,17]:

$$F_{DEP} = 2\pi\epsilon_1 r^3 \text{Re} \left[ \tilde{K}(\omega) \right] \nabla E^2 \quad (1)$$

$$\tilde{K}(\omega) = \frac{\tilde{\epsilon}_2 - \tilde{\epsilon}_1}{\tilde{\epsilon}_2 + 2\tilde{\epsilon}_1} \quad (2)$$

where  $r$  is the radius of the particle,  $\omega$  is the frequency of the applied signal,  $E$  is the electric field,  $\text{Re} \left[ \tilde{K}(\omega) \right]$  is the real part of the Clausius–Mossotti factor, and  $\epsilon_1$  and  $\epsilon_2$  are the dielectric constants of the solvent and particle, respectively; the tilde denotes a complex number. The important point about  $\tilde{K}(\omega)$  is that the positive and negative signs can be reversed depending on the frequency, i.e. it is possible to change an attractive force to a repulsive force within a given region by changing the frequency of the applied electric field. According to Equation (1),  $F_{DEP}$  is dependent on the size of the particles and the gradient of the electric field. For a small particle (typically less than 1  $\mu\text{m}$ ), the effective  $F_{DEP}$  needed to assemble a particle is the force required to overcome the dispersion forces arising from Brownian motion [16,18]. Particle assembly by DEP has been observed in colloidal particles [19], biological cells [20] and protein molecules [16,18,21] by optical microscopy and

fluorescent microscopy. Recently, DEP has been mentioned in studies involving LC-TEM [22], but phenomena related to DEP, such as particle assembly, have not been observed in LC-TEM. By introducing this particle-assembly technique into LC-TEM, it should be possible to assemble particles in a liquid and to increase their concentration locally. Recently, thanks to the development of microelectromechanical system technologies, disk-like proteins with a diameter of 11 nm and a thickness of 6 nm have been experimentally assembled between triangular electrodes with a gap of about 1  $\mu\text{m}$  under a fluorescence microscope [18]. If protein molecules could be assembled around electrodes by using this technique in LC-TEM, this might be an effective method for inducing crystallization of the protein around the electrodes. However, to achieve sufficient assembly of protein molecules, it would be necessary to design a new chip with electrodes having a narrow gap of around 1  $\mu\text{m}$ .

In the present study, instead of protein molecules, we used colloidal particles of a submicron diameter in conjunction with a commercially available chip containing electrodes, and we applied an alternating current (ac) electric field to the electrodes and investigated the resulting phenomena in the liquid cell by phase-contrast optical microscope (PCM). We then attempted to observe the behaviors of colloidal particles by TEM. In addition to testing this system for TEM applications, we also found that it might also be useful as a tool for fabricating two-dimensional patterns in colloids.

## Experimental

We used a commercially available liquid cell for *in situ* liquid TEM observation (Fig. 1a) equipped with an electrode to observe the behavior of colloidal dispersions in an inhomogeneous electric field by optical microscopy and TEM. Two types of liquid-cell holders were used: an external liquid-cell holder (ex-holder) for observation by optical microscopy (Fig. 1b) (Protochips, Inc., Morrisville, NC) and another for observation by TEM (Fig. 1c) (Protochips).

### Liquid cell

The structure of the liquid cell is shown schematically in Fig. 1a. The liquid cell consisted of two silicon chips of different sizes and a perfluoroelastomer gasket. The Si chip was equipped a 50 nm-thick amorphous silicon nitride ( $\text{a-SiN}_x$ ) membrane that served as an electron-transparent observation window, and which separated the high-vacuum sample chamber of the electron microscope from the liquid sample. The larger Si chip was equipped with a platinum electrode on the electron-transparent area of the liquid cell (Fig. 1d and e) (Protochips). Although three circuits were present on the large Si chip, we used only the circuit with the Pt electrode. The other circuits and the metal parts of the holder were connected to the ground. Both the small and large chips had 500 nm spacers so that the thickness of the liquid sample in the observation field was more than 1  $\mu\text{m}$  in total. Note that the distance between the two Si substrates was controlled by the spacers, but the thickness of these spacers did not correspond to that of the liquid sample, which was usually thicker than the combined thickness of the spacers [23]. This was because the window usually bulged due to the pressure difference across the membrane. This bulging was not only due to the vacuum present in the electron microscope but also due to the increase in the

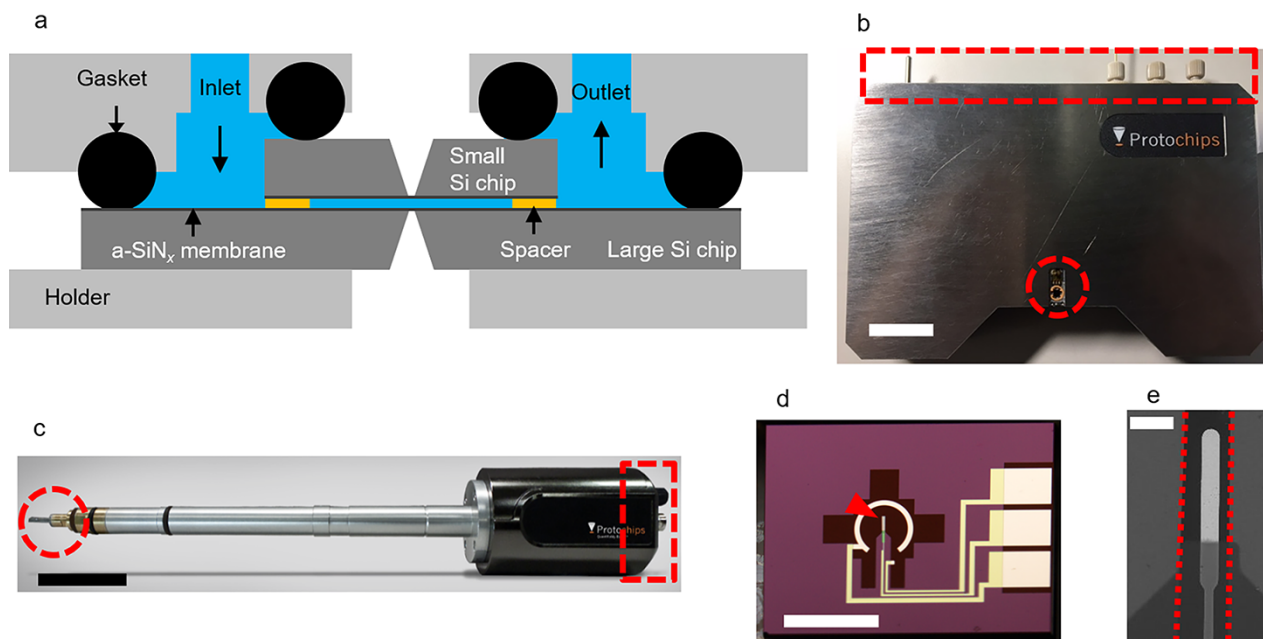


**Fig. 1.** Liquid cell and liquid-cell holders. The design of the liquid cell used in this study is shown schematically in (a); this is not to scale. This liquid cell was assembled by using liquid-cell holders for optical microscopy (b) and for TEM (c). In (b) and (c), the areas enclosed by circles with dashed lines are the regions where the liquid cell was assembled, and the areas enclosed by rectangles with dashed lines show the ports where electrical signals were applied and where the sample liquid was injected into and ejected from the liquid cell. Photograph (d) shows a large Si chip equipped with a Pt electrode, indicated by the red arrowhead. This electrode was connected to a tungsten circuit to permit the application of the electrical signal. The electrode was on a-SiNx membrane, and the area between the two dotted lines in (e) was the area observable by TEM. The scale bars are 2 cm (b), 5 cm (c), 2 mm (d) and 50  $\mu\text{m}$  (e).

internal pressure when the liquid sample was pushed out by the syringe pump. After the cell had been assembled, the liquid sample was introduced into the liquid cell by injection with a syringe pump. During the observations, the liquid sample was continuously introduced into the cell at a flow rate of 2  $\mu\text{L}/\text{min}$  by the action of the syringe pump.

### Samples

Colloidal dispersions of 500 nm-diameter particles of polystyrene (PS; Polybead Polystyrene Microspheres, 500 nm,  $3.64 \times 10^{11}$  particles/mL; Polysciences Inc., Warrington, PA) and silica (Sicstar, Silica Microsphere, Plain, 500 nm,  $3.8 \times 10^{11}$  particles/mL; micromod Partikeltechnologie GmbH, Rostock) were diluted 100 times with ultrapure water for use as the liquid samples. Both these liquid samples were used for observation by PCM, whereas only the liquid dispersion of silica particles was used for TEM observations. Because of the small difference in density between water (density  $\approx 1.0 \text{ g}/\text{cm}^3$ ) and PS particles (density  $\approx 1.05 \text{ g}/\text{cm}^3$ ), the PS particles could not be detected by TEM. In the case of silica, the density of the particles was  $\sim 2.0 \text{ g}/\text{cm}^3$ .

### Alternating current signal and determination of its conditions

We used a function generator (33500B; Keysight Technologies, Santa Rosa, CA) to supply an ac signal to the Pt electrode. The other circuits were connected to the ground (Fig. 1d). In this experiment, the frequency of the applied signal is an important factor in determining the strength and direction of  $F_{DEP}$ . This is because the definition of the Clausius–Mossotti

factor (equation 2) includes the dielectric constants of the solvent and particle, and these are frequency dependent. In this experiment, it was desirable to have a large positive Clausius–Mossotti factor to achieve a strong attractive force between the particle and the electrode. However, if the frequency was excessively low, unwanted effects such as Joule heating and chemical reactions around the electrode, which are the characteristic features of direct currents, would occur. Therefore, the ideal conditions for our experiment is a large Clausius–Mossotti factor and as high a frequency as possible. We experimentally determined the appropriate frequency conditions for PS and silica by varying the frequency (details not shown), and we found that the optimum frequencies of the applied sinusoidal ac signals were 100 and 500 kHz for the PS and silica particles, respectively. The applied voltage was 10  $V_{p-p}$ , which is the maximum value for the device.

### Microscopes and cameras

For *in situ* observation of the behavior of the particles by optical microscopy, we used a PCM (IX-71; Olympus Corp., Tokyo) with a 40 $\times$  objective lens (LCPlanFl 40 $\times$ ; Olympus Corp.). A CMOS camera (UI-3180CP-C; IDS Imaging Development Systems GmbH, Obersulm) was used to obtain video recordings *in situ*. For the *in situ* observations by TEM, we used a field-emission transmission electron microscope (JEM-2100 F; JEOL Ltd., Tokyo) operated at an acceleration voltage of 200 kV. A CMOS camera (FLASH CAMERA; JEOL Ltd.) was used to record the images for the *in situ* TEM observations.

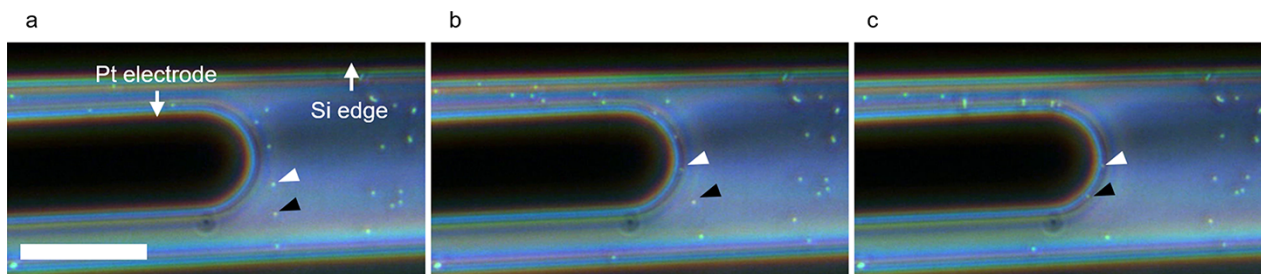


**Fig. 2.** A series of PCM images showing trapping of PS particles on the electrode by DEP. This event is the same as that shown in Video 1. The black rod with the rounded tip extending from the left to the center of the image is the Pt electrode. The boundaries between the Si and the window are visible in the top and bottom of the image, and the black areas are Si. The applied sinusoidal ac signal had a frequency of 100 kHz and a voltage of  $10 V_{p-p}$ . These images were taken 0 (a), 0.1 (b) and 0.4 s (c) after the application of the signal. The colloidal particles indicated by white and black arrowheads were attracted to and trapped on the Pt electrode. The particles that were not moving lost their ability to disperse and were adsorbed on the window. The scale bar is  $20 \mu\text{m}$  (a).

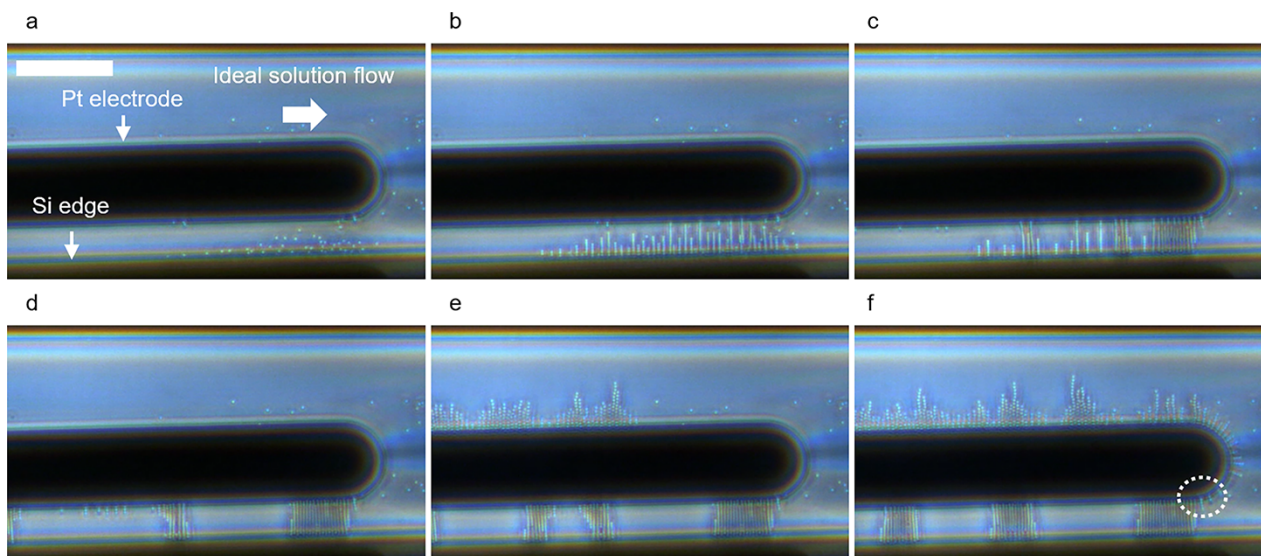


**Fig. 3.** A series of PCM images showing the formation of PS pearl chains and their accumulation. This event is the same as that shown in Video 2. The applied sinusoidal ac signal had a frequency of 100 kHz and a voltage of  $10 V_{p-p}$ . The signal was applied as 0 s and the images were recorded at 0 (a), 0.1 (b), 1 (c), 10 (d), 20 (e) and 26 s (f). Immediately after the application of the signal (b), pearl chains formed, bridging the Pt electrode and Si in the direction along the electric field. The chains that formed gradually moved to the tip of the electrode. Finally, they appeared to move along the edge of the electrode toward the area enclosed by the white dotted ellipse. Some of the accumulated pearl chains did not move because their movement was obstructed by immobile particles. The scale bar is  $20 \mu\text{m}$  (a).

## Results and discussion

### PS particles in an ac electric field observed by PCM using the *ex situ* holder

A characteristic example of the effect of DEP on 500 nm PS particles is shown in Fig. 2 and Video 1. Individual PS particles dispersing with and without Brownian motion were observed. The particles that showed no Brownian motion were those that had been physically adsorbed on the a-SiN<sub>x</sub> membrane. When an electric field was applied, the particles with Brownian motion were immediately attracted to the tip of the electrode and trapped on its surface. The particles without Brownian motion did not move. When the signal was turned off, the particles that had been trapped near the electrode moved away from it with Brownian motion. These observations showed that the force produced by the DEP was sufficient to cause the assembly of the particles when a signal was applied to the electrode in our experimental setup.

When large numbers of particles were present between the electrodes, they interacted with each other to form a chain-like structure referred to as a ‘pearl chain’ [19] (Fig. 3, Video 2). The pearl chain is formed as a result of the dipole–dipole interactions resulting from the dipole moments induced in the particles by the applied electric field [19,21]. The induced dipole creates an additional electrostatic field around the particles that results in an attractive force between particles in the direction of the electric field and a repulsive force perpendicular to the electric field [24]. As a result, the particles assemble in the direction of the electric field, leading to the formation of a pearl chain structure. The observed pearl chain formed a bridge between the Pt electrode and the Si edge, confirming that a potential difference existed between the Pt electrode and the Si edge (shown in schematically [Supplementary Fig. S1](#)). The resulting pearl chains then moved toward the electrode and accumulated near its tip (Fig. 3, Video 2). The movement of the pearl chains from the root to the tip of the electrode was due to the unidirectional and continuous

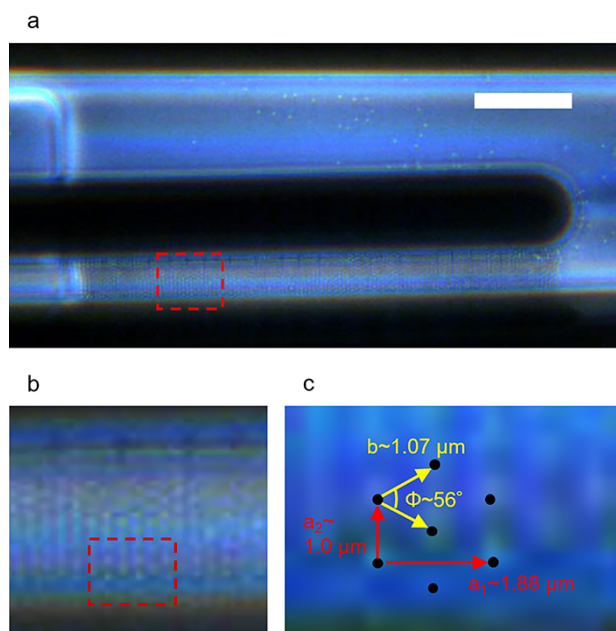


**Fig. 4.** Formation of a PS colloidal crystal through accumulation of pearl chains. Enlarged images of the rectangular areas enclosed by red dashes in (a) and (b) are shown in (b) and (c), respectively. The pattern formed by the colloidal particles in the enlarged image (c) showed that they were regularly arranged in a centered rectangular system of a Bravais lattice in two dimensions with the lattice parameters shown in the image. The scale bar is 20  $\mu\text{m}$  (a).

solution flow because we did not observe any movement of pearl chains when we performed the same experiment without solution flow (Video 3). It is therefore likely that the formed pearl chains were moved to the tip by the solution flow and were attracted to the electrode as they travelled around the tip of the electrode, accumulating at the point where the electric field gradient was greatest (Fig. 3f).

When sufficient particles had accumulated, the pearl chains joined together to form a periodic lattice pattern, suggestive of the formation of a crystal (Fig. 4). The lattice distances were measured, and the crystal system was characterized as centered rectangular in a Bravais lattice in two dimensions with the closest lattice spacing parallel to the direction of the electric field and a slightly wider spacing perpendicular to the field (Fig. 4; the lattice parameters are  $a_1 \approx 1.88 \mu\text{m}$ ,  $a_2 \approx 1.0 \mu\text{m}$ ,  $b \approx 1.07 \mu\text{m}$ , and  $\Phi \approx 56^\circ$ ). This structure probably originates from the difference between the particle–particle interactions parallel to the electric field and those perpendicular to it, caused by the difference between the attractive and the repulsive interparticle potentials in the directions parallel and perpendicular to the electric field, respectively. This difference in the forces experienced by the particles depending on their direction could potentially create a variety of assembly patterns [25]. In particular, because the thickness of the liquid layer was limited to around 1  $\mu\text{m}$ , by selecting colloids of appropriate size, it might be possible to obtain two-dimensional colloidal crystals of possible use in such applications as colloidal lithography [26]. It would be interesting to investigate the types of patterns formed on changing the signal applied to the electrode and the size of the colloidal particles.

### Silica particles in the ac electric field observed by PCM and TEM

Because the densities of PS and water are very similar, it is difficult to observe PS particles in water by TEM. We therefore conducted the same experiment by using silica particles, which have about twice the density of PS. First, we observed the silica particles by PCM using the ex-holder at a signal frequency of 500 kHz, where the silica particles responded (Fig. 5 and Video 4). Note that because the silica particles were more difficult to observe than the PS particles, a green filter was used to improve their visibility. The reason for the difficulty in visualizing the silica particle is probably because they were smaller than 500 nm (Supplementary Fig. S2); however, this does not significantly affect the conclusions discussed below. Under these conditions, the silica particles formed pearl chains that assembled between the electrodes in a manner similar to that of the PS particles. We then conducted the same experiment to observe the silica particles assembling around the electrodes by TEM using the TEM holder. We expected to obtain similar results to those from PCM, but the phenomena observed by TEM (Fig. 6 and Video 5) differed from those observed by PCM, even though the experimental setup was the same except for the liquid-cell holder. Before irradiation by the electron beam to image the liquid cell, the liquid-cell holder was inserted into the TEM and a signal was applied to the electrode. In this procedure, we expected that the silica particles already assembled in the liquid cell at the moment of electron-beam irradiation. However, no assembled particles were observed immediately after the start of the observations, and only a few immobile particles were observed (Fig. 6b); however, on continuing the observations, pearl chains trapped in the observation area were eventually observed (Fig. 6c and d). These results indicated that a different situation existed in the TEM compared with that in the PCM.

Next, we will discuss the phenomena observed by TEM. First, a signal was definitely applied to the electrode, because pearl chains formed radially from the tip of the electrode along the direction of the electric field; however, no assembled particles were observed immediately after starting the observations. We speculate that the electric-field gradient created by the applied signal was insufficient to trap the particles on the tip of the electrode. There are two main reasons why the applied signal was weaker at the tip of the electrode in TEM: crosstalk and wrinkling of the window. Crosstalk is a phenomenon that occurs when an ac signal is applied to one of two adjacent parallel conducting wires and the signal is transferred to the second conducting wire. Crosstalk is unique to ac signals, especially those of radio frequency, and it becomes more pronounced as the frequency increases. When crosstalk occurs, the signal reaching the end of the wire (in our case, the Pt electrode in the liquid cell) is attenuated compared with the applied signal. This acts to reduce the electric field gradient. Crosstalk can generally be prevented by using coaxial cables. However, because the liquid cell holders were not designed to use ac signals, coaxial cables were not employed. We therefore consider that the effect of crosstalk is a plausible explanation for the weakening of the DEP forces. In addition, crosstalk becomes more pronounced as the conducting wires become longer and the distance between them becomes smaller. The conducting wires of the TEM holder

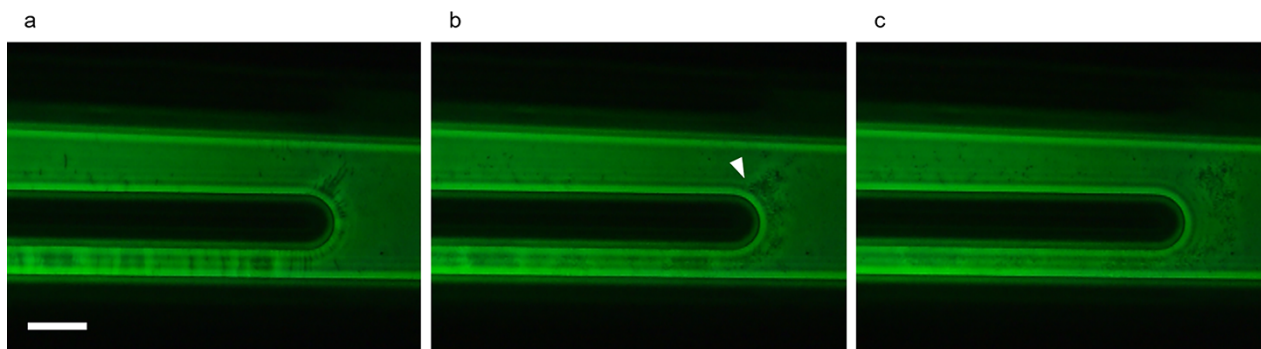


**Fig. 5.** A series of PCM images of trapped silica particles and their separation. This event is the same as that shown in Video 4. The applied sinusoidal ac signal had a frequency of 500 kHz and a voltage of 10 V<sub>p-p</sub>. The silica particles were trapped, and pearl chains were formed when the signal was applied (a). They subsequently separated from the electrode (indicated by a white arrowhead) when the signal was stopped (b) and dispersed 3 s after stopping the signal (c). These images were taken by using a green interference filter. The scale bar is 20 μm.

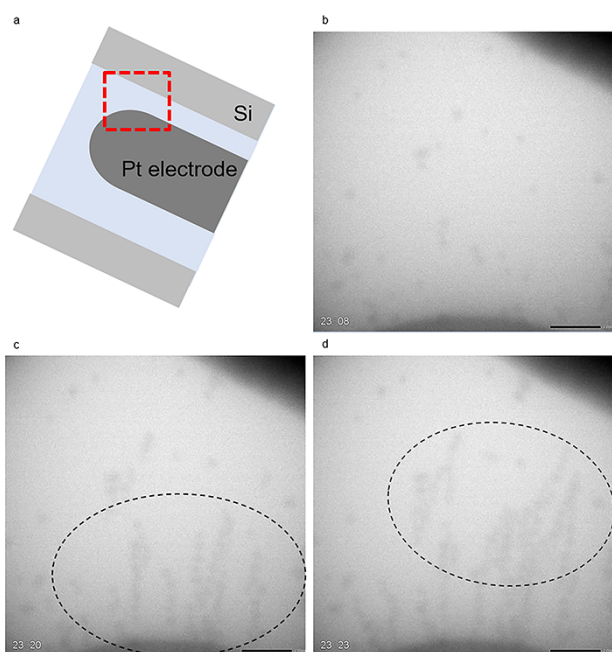


**Fig. 6.** A series of LC-TEM images of silica particles in an ac electric field. The sinusoidal ac signal had a frequency of 500 kHz and a voltage of 10 V<sub>p-p</sub>. The observation area was that enclosed by the red dashed rectangle in the schematic illustration of the liquid cell (a). Immediately after starting the observations, immobile silica particles adsorbed on the a-SiN<sub>x</sub> window were observed, but no pearl chains were observed (b). Twelve (c) and 15 s (d) after (b), pearl chains were trapped between the electrode and the edge of Si in the area enclosed by the black dashed circle in (c) and (d). This event is the same as that shown in Video 5. The scale bar is 2 μm.

appeared to be longer than those of the *ex situ* holder and, consequently, the signal applied to the tip of the electrode was weaker in the TEM holder. For reference, we used an inductance–capacitance–resistance meter (U1733C; Keysight Technologies, Santa Rosa, CA) to measure the capacitance, which is an indicator of extent of crosstalk. The capacitance of the TEM holder (~270 pF) was found to be larger than that of the *ex situ* holder (~100 pF), indicating that crosstalk is more likely to have occurred in the TEM holder. To investigate this in detail, it would be necessary to disassemble the holders to determine the type of conducting wires used in the TEM holder, their length, and their separation distance.

Note that neither of the holders used in this study was designed for use with radio-frequency signals, i.e. no countermeasures to minimize crosstalk were present. The best way to prevent crosstalk would be to use coaxial cables for the conducting wires. Another practical answer would be to fabricate Si chips with a smaller distance between the electrodes, so as to increase the electric-field gradient around the tip of the electrodes, even from weak applied signals.

The second possibility is that wrinkles in the window (Supplementary Fig. S3) might have disturbed the electric field around the electrodes. Wrinkles were observed in the window of the liquid cell in the TEM holder, whereas no wrinkles were present on the membrane in the *ex situ* holder (Supplementary Fig. S3). The wrinkles in the TEM holder were caused by stress on the a-SiN<sub>x</sub> film during the process of holding the Si chips at the appropriate torque (~1 cN·m), and the appearance of wrinkles is difficult to avoid because this is an intrinsic problem associated with the design of the holder. It is likely that placing a wrinkled a-SiN<sub>x</sub> film between the Pt electrode and Si chip will disturb the electric field generated between them. However, it is not easy to determine the actual three-dimensional structure around the electrode. One way to understand this effect would be to use another TEM holder with wrinkles of different shapes in the window.

The last issue involved in the TEM observations was the formation of the pearl chains several seconds after starting the observations. This time lag might have occurred because the electron beam destroyed the structure of the water present in the electric double layer around the particles. This double layer is responsible for the electrostatic repulsive force of the colloidal particles. Therefore, the destruction of the structure facilitates the trapping of the particles because of a loss of their ability to repel one another. On the basis of our results, we concluded that differences in the observations were mainly due to the difference in the design of the holders (Fig. 1b and c). Solving these issues should lead to the establishment of a technique for manipulating particles by using electrodes in LC-TEM and in an expansion of the range of experiments that can be performed with LC-TEM.

## Concluding remarks

We investigated the manipulation of particles by dielectrophoresis in LC-TEM as a method for changing the conditions in the observation area. First, we performed

observations by using PCM to determine which phenomena occurred in the existing system; we then performed similar experiments using TEM and we showed that phenomena observed by PCM were not observed in TEM. Based on these observations, we identified the difference in the design of the holders as a factor responsible for the difference in the results of observations by the two methods. Electrical crosstalk and the effect of wrinkles in the observation window are two possible explanations for these differences. To overcome the problem of using the existing TEM holder, we propose to use a Si chip with a narrower gap between the electrodes to increase the electric-field gradient around the electrodes. We hope that this will be beneficial for the further developments in the dielectrophoretic manipulation of particles in LC-TEM to expand the range of experiments possible by using this method.

## Acknowledgements

We thank Dr. J. Nozawa (Tohoku University) and Mr. S. Mori (Hokkaido University) for technical supports.

## Funding

This work was supported by the GIMRT Program of the Institute for Materials Research, Tohoku University (Proposal No. 20K0038) and by JSPS KAKENHI (grants numbers JP20H02580 and JP20H05657).

## Supplementary data

[Supplementary data](#) are available at *Microscopy* online.

## References

1. de Jonge N and Ross F M (2011) Electron microscopy of specimens in liquid. *Nat. Nanotechnol.* 6: 695–704.
2. de Jonge N, Houben L, Dunin-Borkowski R E, and Ross F M (2019) Resolution and aberration correction in liquid cell transmission electron microscopy. *Nat. Rev. Mater.* 4: 61–78.
3. Woehl T J, Evans J E, Arslan I, Ristenpart W D, and Browning N D (2012) Direct *in situ* determination of the mechanisms controlling nanoparticle nucleation and growth. *ACS Nano* 6: 8599–8610.
4. Loh N D, Sen S, Bosman M, Tan S F, Zhong J, Nijhuis C A, Král P, Matsudaira P, and Mirsaidov U (2017) Multistep nucleation of nanocrystals in aqueous solution. *Nat. Chem.* 9: 77–82.
5. Nielsen M H, Aloni S, and De Yoreo J J (2014) *In situ* TEM imaging of CaCO<sub>3</sub> nucleation reveals coexistence of direct and indirect pathways. *Science* 345: 1158–1162.
6. Smeets P J M, Cho K R, Kempen R G E, Sommerdijk N A J M, and De Yoreo J J (2015) Calcium carbonate nucleation driven by ion binding in a biomimetic matrix revealed by *in situ* electron microscopy. *Nat. Mater.* 14: 394–399.
7. Yamazaki T, Kimura Y, Vekilov P G, Furukawa E, Shirai M, Matsumoto H, Van Driessche A E S, and Tsukamoto K (2017) Two types of amorphous protein particles facilitate crystal nucleation. *Proc. Natl. Acad. Sci. U. S. A.* 114: 2154–2159.
8. Cookman J, Hamilton V, Price L S, Hall S R, and Bangert U (2020) Visualising early-stage liquid phase organic crystal growth *via* liquid cell electron microscopy. *Nanoscale* 12: 4636–4644.
9. Patterson J P, Abellan P, Denny M S Jr, Park C, Browning N D, Cohen S M, Evans J E, and Gianneschi N C (2015) Observing the growth of metal–organic frameworks by *in situ* liquid cell transmission electron microscopy. *J. Am. Chem. Soc.* 137: 7322–7328.
10. Ou Z, Wang Z, Luo B, Luijten E, and Chen Q (2020) Kinetic pathways of crystallization at the nanoscale. *Nat. Mater.* 19: 450–455.
11. Schneider N M, Norton M M, Mendel B J, Grogan J M, Ross F M, and Bau H H (2014) Electron–water interactions and implications for liquid cell electron microscopy. *J. Phys. Chem. C* 118: 22373–22382.
12. Ambrožič B, Prašnikar A, Hodnik N, Kostevšek N, Likozar B, Žužek Rožman K, and Šturm S (2019) Controlling the radical-induced redox chemistry inside a liquid-cell TEM. *Chem. Sci.* 10: 8735–8743.
13. Yuk J M, Zhou Q, Chang J, Ercius P, Alivisatos A P, and Zettl A (2016) Real-time observation of water-soluble mineral precipitation in aqueous solution by *in situ* high-resolution electron microscopy. *ACS Nano* 10: 88–92.
14. Yamazaki T and Kimura Y (2021) Radiolysis-induced crystallization of sodium chloride in acetone by electron beam irradiation. *Microsc. Microanal.* 27: 459–465.
15. Pohl H A (1951) The motion and precipitation of suspensions in divergent electric fields. *J. Appl. Phys.* 22: 869–871.
16. Washizu M, Suzuki S, Kurosawa O, Nishizaka T, and Shinohara T (1994) Molecular dielectrophoresis of biopolymers. *IEEE Trans. Ind. Appl.* 30: 835–843.
17. Jones T B (1995) *Electromechanics of Particles*, (Cambridge University Press, Cambridge).
18. Hölzel R, Calander N, Chiragwandi Z, Willander M, and Bier F F (2005) Trapping single molecules by dielectrophoresis. *Phys. Rev. Lett.* 95: 128102.
19. Velev O D and Bhatt K H (2006) On-chip micromanipulation and assembly of colloidal particles by electric fields. *Soft Matter* 2: 738–750.
20. Chiou P Y, Ohta A T, and Wu M C (2005) Massively parallel manipulation of single cells and microparticles using optical images. *Nature* 436: 370–372.
21. Pethig R (2017) Review—where is dielectrophoresis (DEP) going? *J. Electrochem. Soc.* 164: B3049–B3055.
22. Leenheer A J, Sullivan J P, Shaw M J, and Harris C T (2015) A sealed liquid cell for *in situ* transmission electron microscopy of controlled electrochemical processes. *J. Microelectromech. Syst.* 24: 1061–1068.
23. Holtz M E, Yu Y, Gao J, Abruña H D, and Muller D A (2013) *In situ* electron energy-loss spectroscopy in liquids. *Microsc. Microanal.* 19: 1027–1035.
24. Wang X-B, Huang Y, Gascoyne P R C, and Becker F F (1994) Particle dipole-dipole interaction in AC electric fields (cellular application). In: *Proc. 16th Ann. Int. Conf. IEEE Engineering in Medicine and Biology Society*, Vol. 2, pp 774–775 (Baltimore, MD, USA).
25. Yethiraj A (2007) Tunable colloids: control of colloidal phase transitions with tunable interactions. *Soft Matter* 3: 1099–1115.
26. Zhang J, Li Y, Zhang X, and Yang B (2010) Colloidal self-assembly meets nanofabrication: from two-dimensional colloidal crystals to nanostructure arrays. *Adv. Mater.* 22: 4249–4269.